ADVANCED ENERGY MATERIALS
www.advenergymat.de

Unprecedented Aqueous Solubility of TEMPO and its Application as High Capacity Catholyte for Aqueous Organic Redox Flow Batteries

Eduardo Pedraza, Carlos de la Cruz, Andreas Mavrandonakis, Edgar Ventosa, Rubén Rubio-Presa, Roberto Sanz, Sirugaloor Thangavel Senthilkumar, Paula Navalpotro,* and Rebeca Marcilla**

Despite the excellent electrochemical properties of non-functionalized 2,2,6,6-tetramethylpiperidine-1-oxyl (TEMPO), its use in aqueous organic redox flow battery (AORFB) is hindered to date due to its insolubility in water. However, in this study, an unprecedented solubility of 5.6 M is demonstrated in an aqueous solution of lithium bis(trifluoromethanesulfonyl)imide (LiTFSI), which is 80 times higher than in water (0.07 M). A computational study reveals that the unique interaction between TEMPO and TFSI is essential to achieve this record solubility. TEMPO catholytes are tested in symmetric flow cells, demonstrating high capacity (23.85 Ah L^{-1}), high material utilization (89%), and robust reversible performance with long-term stability (low capacity fading of 0.082%/day). When paired with sulfonated viologen anolyte ($(SPr_2)V$), an AORFB with low capacity fading over cycling (0.60%/day, 0.048%/cycle) is achieved, constituting the first example of a non-functionalized TEMPO catholyte for AORFB. Notably, this solubilization strategy could be applied to other unexplored chemistries in aqueous electrolytes, leading to the development of new AORFBs.

1. Introduction

Redox flow batteries (RFBs) have unique characteristics, such as decoupled power and energy, safety, and easy scalability, which make them one of the most predominant candidates for large-scale energy storage applications. Indeed, RFBs have the potential to store the excess of electrical energy (from kW to GW) produced from intermittent renewable energies, that is, solar and wind power, and release it when required.[1] Among all the different RFB technologies, all-vanadium RFBs and zinc-bromide RFBs are the most mature technologies.[2] However, those RFBs commonly use expensive, highly corrosive, acidic, and toxic electrolytes, thus preventing their wide expansion into the market. Hence, in recent years, aqueous organic redox flow batteries (AORFBs) have been considered one sustainable alternative since the replacement of vanadium and bromide species by organic redox molecules offers significant advantages such as high abundance in nature, safety, and lower cost to make cost-effective RFBs.[2]

So far, several families of organic redox molecules, such as quinones, viologens, phenazynes, quinoxalines, alloxazines, phthalimides, and nitroxide radicals, have been investigated as active species in aqueous and non-aqueous RFBs.[3–9] Among the large number of redox molecules, 2,2,6,6-tetramethylpiperidine-1-oxyl (TEMPO) has been considered one of the most promising candidates to be used as catholytes in RFB. TEMPO is a heterocyclic nitroxide radical compound that has the favorable features of low cost, high specific capacity determined by their small molecular weight, easy accessibility (commercially available), high redox potential, high redox reversibility, fast redox kinetics, and excellent chemical and electrochemical stability. However, due to the low solubility of TEMPO in water (≈70 mM),[10] its use as catholyte has been restricted to non-aqueous electrolytes where TEMPO is highly soluble (up to 2 M in 2.3 M $LiPF_6$ /EC-PC-EMC).[11,12]

A common approach to increase the solubility of TEMPO in aqueous electrolytes is through chemical functionalization of the parent TEMPO molecule. For instance, 4-hydroxy-TEMPO is a 4-substituted TEMPO derivative that was first employed as a neutral aqueous catholyte by Prof. Wang in 2016.[13] This molecule

E. Pedraza, C. de la Cruz, A. Mavrandonakis, S. T. Senthilkumar, P. Navalpotro, R. Marcilla
Electrochemical Processes Unit
IMDEA Energy
Avenida Ramón de la Sagra 3, Móstoles 28935, Spain
E-mail: senthilkumar.sirugaloor@imdea.org; paula.navalpotro@imdea.org; rebeca.marcilla@imdea.org
E. Ventosa, R. Rubio-Presa, R. Sanz
Department of Chemistry
University of Burgos
Pza. Misael Bañuelos s/n, Burgos E-09001, Spain
The ORCID identification number(s) for the author(s) of this article can be found under https://doi.org/10.1002/aenm.202301929

DOI: 10.1002/aenm.202301929

presented a solubility of ≈2.11 м in water, but decreased up to 0.5 м when NaCl supporting salt was added. In addition, when paired with methylviologen anolyte, the resultant RFB showed modest long-term stability, especially at high 4-OH-TEMPO concentrations, due to the detrimental side reaction through the self-catalyzed oxidation of the alcohol.[13,14] A similar derivative is the 4-amino-TEMPO substituting the OH by a NH_2 group. Although the solubility was as high as 4.80 м in 0.5 м KCl, the electrochemical performance was even poorer than that for 4-OH-TEMPO, losing half of its capacity in only 40 cycles.[15]

It is important to remark that the modest chemical/electrochemical stability of organic molecules (especially compared with their inorganic counterparts) is a limiting factor for the development of AORFB since it affects directly the lifespan of RFB and their levelized cost (kWh/cycle).[16] Consequently, prominent effort has been also made in the synthesis of new TEMPO derivatives to improve both their solubility and their chemical stability. For instance, *N*,*N*,*N*-2,2,6,6-heptamethylpiperidinyl oxy-4-ammonium chloride (TEMPTMA),[17] 4-[3-(trimethylammonio)propoxy]–2,2,6,6-tetramethylpiperidine-1-oxyl chloride (TMAP-TEMPO),[18] and *N*1, *N*1, *N*1, *N*3, *N*3, 2, 2, 6,6-nonamethyl-*N*3-(piperidinyloxy)propane-1,3-bis(ammonium) dichloride (N_2-TEMPO)[19] have been recently proposed as neutral pH catholyte for AORFB. While promising results were obtained in terms of solubility (up to 4.6 м in deionized water) and long-term electrochemical performance compared to 4-OH-TEMPO and 4-amino-TEMPO, the synthesis of these TEMPO derivatives involves multistep synthetic routes, resulting in more time and energy-consuming processes compared to bare TEMPO, which can be synthesized on a large scale and is commercially accessible. Moreover, the electrochemical performance of the functionalized TEMPO derivatives is usually worse than the pristine TEMPO.[15] Therefore, alternative strategies to increase the solubility of TEMPO while keeping the excellent reversibility and long-term cyclability of pristine TEMPO are required to develop high energy density catholytes at a low levelized cost of energy.

In this work, we report a radically different approach to developing a high-capacity aqueous catholyte based on pristine TEMPO. Instead of modifying the structure of TEMPO by adding functionalities that could potentially lead to molecular decomposition, our pioneering strategy is to promote the solubility of pristine TEMPO by changing the formulation of the supporting electrolyte. We demonstrate here that pristine TEMPO features a record solubility in aqueous electrolyte (up to 5.6 м (9.4 kg L^{-1}) of TEMPO in 5 м lithium bis(trifluoromethanesulfonyl)imide (LiTFSI)) corresponding to a potentially theoretical volumetric capacity of 150 $Ah/L_{catholyte}$. This extraordinarily high TEMPO solubility is due to the unique interaction of TEMPO with the TFSI anion. Using molecular dynamics (MD), we shed light on this phenomenon by scrutinizing the coordination sphere of the different components of the electrolytes. Moreover, the electrochemical performance of pristine TEMPO in this supporting electrolyte is demonstrated to be excellent with a reversible redox potential (0.57 vs SHE), fast kinetics ($k_0 = 0.018$ $cm^{-1}s$, $D_{eff} = 8.9 \times 10^{-7}$ cm^2 s^{-1}), and high chemical and electrochemical stability. Then, the feasibility of practical TEMPO-based catholytes (0.1, 0.5, and 1 м in 4 м LiTFSI) was studied in symmetric flow cells. The TEMPO catholyte with a concentration of 1 м showed a high capacity of 23.6 Ah L^{-1} corresponding to 88% of material utilization, excellent Coulombic efficiency (CE) (>99.5%), and long-term stability (0.014% per cycle (0.082% per day). Finally, by pairing this catholyte with a viologen-derivative anolyte we assemble a battery (0.5 м TEMPO/0.25 м $(SPr)_2$ V RFB) with an open circuit voltage (OCV) of 1.08 V and extremely high capacity retention rate of 99.952% per cycle over 285 consecutive cycles (≈552 h). This constitutes a temporal capacity fade rate of 0.60% per day, being is one of the lowest ever reported for neutral aqueous RFB.

2. Results and Discussion

2.1. Solubility of TEMPO in Aqueous Electrolytes Having Different Supporting Salts

Although the functionalization has been demonstrated to be an adequate approach to increase the solubility of TEMPO derivatives in pure water, the necessary presence of supporting salts is highly detrimental to the solubility of such compounds. For example, the initial solubility of 2.1 м for the 4-OH-TEMPO in pure water decreases to 0.69, 0.5, and 0.33 м in LiCl, NaCl, and Na_2SO_4-based supporting electrolytes, respectively.[15] Similarly, other TEMPO derivatives, such as 4-N_2-TEMPO, TEMPTMA, and 4-oxo-TEMPO, also experience the same decreasing trend in solubility for aqueous electrolytes containing supporting salts (see Table S1 and Figure S6, Supporting Information). Contrary, in this work, we demonstrate that pristine nitroxide radical TEMPO, insoluble in pure water, become highly soluble when certain salts are used as supporting electrolyte. Table S2, Supporting Information, shows that the solubility of TEMPO dramatically increased (by 3 orders of magnitude) when LiTFSI or NaTFSI were used as supporting salts whereas the solubility slightly decreased in the presence of the other supporting Li-salts. In addition, it was found that the solubility of TEMPO increased with increasing LiTFSI concentration, from 2.2 kg L^{-1} (≈4.4 м) in 1 м LiTFSI up to 9.4 kg L^{-1} (≈5.6 м) in 5 м LiTFSI (orange bars in **Figure 1**). It should be noticed that, although an apparent independence of TEMPO solubility with the concentration of the supporting electrolyte can be observed in molarity (Figure 1a), this is just derived from the use of volume of solution (salt + solvent), to calculate the molarity. Nevertheless, by defining the solubility as kg L^{-1} (referred to volume of solvent), the increase of TEMPO solubility with LITFSI concentration is clear (Figure 1b) thus demonstrating the dependence of TEMPO solubility with the supporting salt concentration. This large increment in TEMPO solubility with LiTFSI concentration is not largely impacting the molarity due to the significant volume changes in the solution (see Table S3, Supporting Information, for weight and molar composition comparison). Irrefutably, this high solubility in aqueous electrolyte, never reported before for a non-functionalized TEMPO, makes this electrolyte a promising catholyte for AORFB.

In the literature, the solubility of the "non-charged" active species is often used to estimate the theoretical capacity, which would suggest a volumetric capacity of 150 Ah L^{-1} for a solubility of 5.6 м here. However, this approach is not fully rigorous, since the theoretical capacity is ultimately determined by

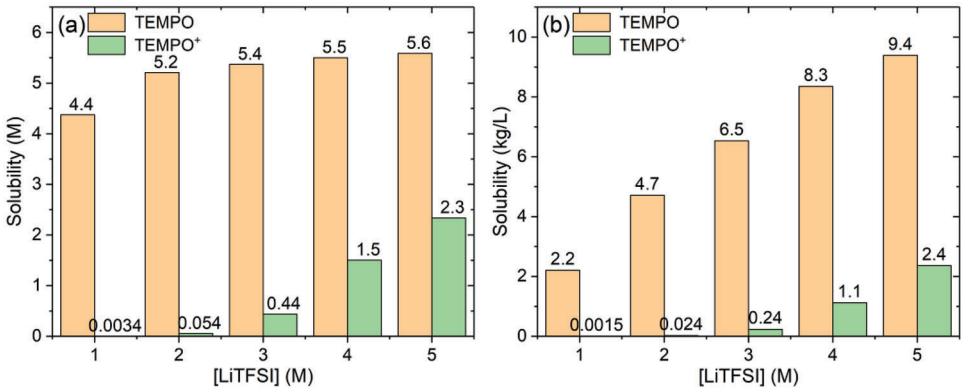

Figure 1. Solubility of nitroxide radical TEMPO (orange) and their oxoammonium cation $TEMPO^+$ (green) in LiTFSI aqueous solutions. a) Solubility in molarity (mol of solute per liters of solution). b) Solubility in kg L^{-1} (kg of solute per liter of solvent).

the solubility of the least soluble species, considering both the charged and uncharged forms of the compound. Unfortunately, the solubility of the charged species is generally overseen in literature, leading to overestimated values of the theoretical capacity. In this work, we also determined the solubility of the corresponding oxidized species, the oxoammonium cation $TEMPO^+$. To obtain $TEMPO^+$, we synthesized and obtained the oxidized $TEMPO^+$-$TFSI^-$ salt and its solubility in LiTFSI-based aqueous electrolytes is depicted in Figure 1 (green bars). Despite being less soluble than TEMPO, the oxoammonium cation $TEMPO^+$ still exhibits high solubility values, with a maximum solubility of 2.4 kg L^{-1} (2.3 м) in 5 м LiTFSI. This demonstrates the potential of the TEMPO–$TEMPO^+$ redox pair in LiTFSI-based aqueous electrolytes as a high-capacity catholyte, with a theoretical capacity as high as ≈61.6 $Ah/L_{catholyte}$, when considering the solubility limit of the oxidized species.

2.2. Computational Studies for Better Understanding TEMPO Solubility

MD simulations were performed in order to rationalize the unusual solubility of nitroxide radical TEMPO and their oxoammonium cation $TEMPO^+$ in LiTFSI-based aqueous electrolytes. MDs were carried out with the GROMACS package[20] for several aqueous systems containing TEMPO or $TEMPO^+$ in the presence of different salts (Table S4, Supporting Information) with different concentrations (Table S5, Supporting Information). After the MDs, the analysis of the coordination environment of TEMPO and $TEMPO^+$ was computed with the radial distribution function (RDF) and coordination number (CN). The details for the computational procedure are described in the EIS (see also Figures S7–S23, Supporting Information).

By visual inspection of the different systems, the MDs show micellar aggregation for TEMPO in all the supporting salts ($LiClO_4$, LiCl, and Li_2SO_4) with the exception of the LiTFSI. **Figure 2**a shows that a stronger coordination of TEMPO with the TFSI anions is observed, compared to the other anions, in which the solubility of TEMPO is very low. The analysis of the MDs shows that the TEMPO-$TFSI^-$ pair has the highest CN (Figure 2a and Figure S16, Supporting Information), while the TEMPO–TEMPO and TEMPO-Water pairs have the lowest CNs in the presence of the LiTFSI salt (Figure S16, Supporting Information). Upon increasing the concentration of LiTFSI, the CN of TEMPO–TEMPO decreases significantly from a value of 7 to 4.5 and 0.9 for 1, 3, and 5 м LiTFSI, respectively (Figure 2b,c and Figure S17, Supporting Information). Simultaneously, the TEMPO-$TFSI^-$ CN is increasing from a value of 2.1 to 3.2 and 5.2 with increasing concentration of LiTFSI, while the CN of TEMPO-Water remains almost constant (Figure S17, Supporting Information). This means that the unique solubility behavior of TEMPO in LiTFSI-based electrolytes can be attributed to a change in its coordination environment that incorporates more $TFSI^-$ and displaces other TEMPO molecules from its coordination shell. The same trend can be observed in systems containing oxoammonium cation $TEMPO^+$ in electrolytes with increasing LiTFSI concentrations, as shown in Figures S13–S15 and S18, Supporting Information. These results are consistent with the experimentally observed increase in solubility of $TEMPO^+$ in electrolytes with increasing LiTFSI concentrations, as depicted in Figure 1.

Furthermore, these findings can also be supported by analyzing the average interaction energies for both TEMPO and oxidized-$TEMPO^+$. In **Figure 3**, the Lennard–Jones (or Van der Waals dispersions), Coulombic, and total interaction energies are plotted for the most relevant systems for radical and cationic TEMPO. Figure 3a shows that among all the different salts, the strongest interaction energies of the TEMPO are with the TFSI anion (−43.6 $kJmol^{-1}$), followed by the ClO_4^- anion (−11.65 $kJmol^{-1}$) whereas the interactions with the Cl^- and SO_4^{2-} anions are negligible. As shown previously by the RDFs and CN analysis, the hydrophobicity of the $TFSI^-$ anion was found to be the highest among all the studied anions (see Figures S9 and S20, Supporting Information). Moreover, the hydrophobic character of TEMPO explains its insolubility in water. Therefore, the higher affinity between TEMPO and $TFSI^-$ (Figure 3a) can be explained by the hydrophobicity of both compounds. These mutual hydrophobicities induce an affinity between the TEMPO and $TFSI^-$ that is able to compensate for the energy loss by breaking the cluster aggregation of TEMPO and promoting their dissolution. Figure 3b,c reveals that the interactions of both TEMPO and $TEMPO^+$ with the $TFSI^-$ anion increase with the concentration of LiTFSI. This observation confirms the higher affinity of TEMPO and oxidized-$TEMPO^+$ with $TFSI^-$ anion, and how

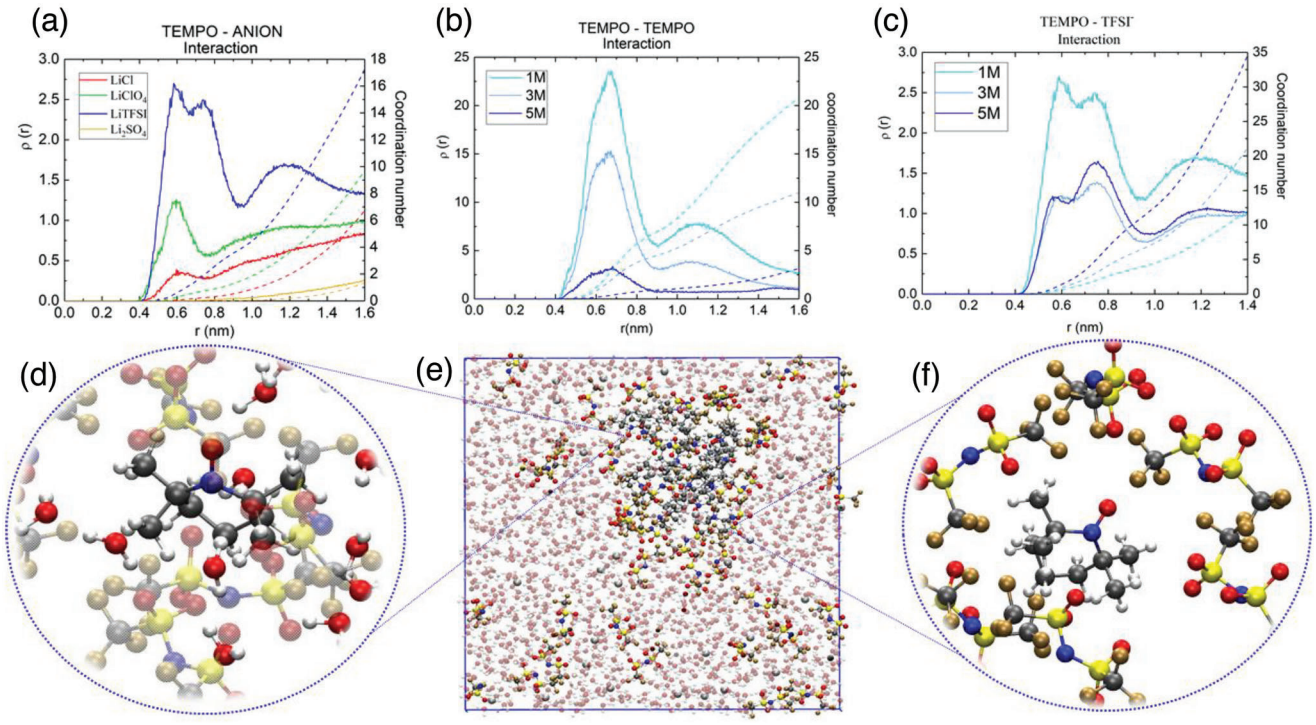

Figure 2. RDFs and CNs for a) TEMPO-Anion pairs in 1 M salt concentration, b) TEMPO–TEMPO interaction, and c) TEMPO-TFSI$^-$ pairs in LiTFSI solutions at different concentrations. d) Snapshot of TEMPO surrounded by water and TFSI$^-$. e) Simulation box for [TEMPO] = 0.3 M with [LITFSI] = 1 M system. f) TEMPO surrounded by TFSI$^-$ (water molecules are omitted for clear visualization).

the presence of LiTFSI can alter the environment of TEMPO in the solution, thus promoting their solubility. Consequently, the solubility trends predicted by the theoretical study for both TEMPO and TEMPO$^+$ in supporting electrolytes with increasing concentrations of LiTFSI are in good agreement with the solubility trends determined experimentally (Figure 1).

2.3. Ionic Conductivity of LiTFSI Supporting Electrolyte

Besides the concentration of active species, other parameters, such as conductivity, should be considered to optimize the electrolyte for an efficient RFB operation. Therefore, the conductivity of LiTFSI aqueous solutions was measured at different concentrations from 1 to 5 M LiTFSI. Figure S24, Supporting Information, shows that the conductivity varied from 37 mS cm^{-1} at 1 M LiTFSI to a maximum of 55 mS cm^{-1} at 2.6 M LiTFSI to decrease again down to 11 mS cm^{-1} at 5 M LiTFSI. Therefore, despite that the highest solubility of TEMPO and oxidized-TEMPO$^+$ was found to be in 5 M LiTFSI (5.6 and 2.3 M, respectively), a concentration of 4 M LiTFSI was selected as the optimum supporting electrolyte formulation since it achieves a trade-off between conductivity (37 mS cm^{-1}) and active species solubility (5.5 and 1.5 M, for TEMPO and TEMPO$^+$, respectively). Therefore, for the subsequent preparation and electrochemical characterization of the electrolytes, a supporting salt concentration of 4 M LiTFSI was employed. As depicted in Figure 1, the maximum solubility of the

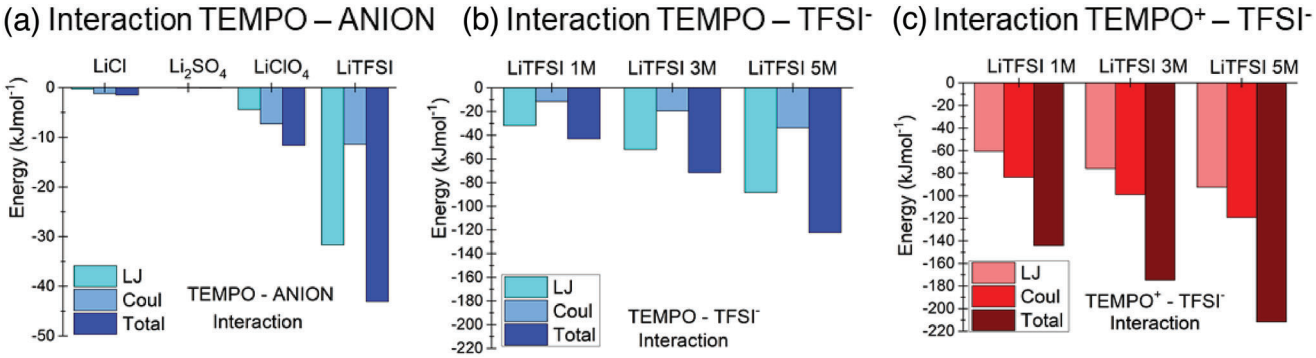

Figure 3. Lennard–Jones (LJ), Coulombic, and total interaction energies for a) TEMPO-Anion pairs, b) TEMPO-TFSI$^-$ pairs, and c) oxidized-TEMPO$^+$-TFSI$^-$ pairs.

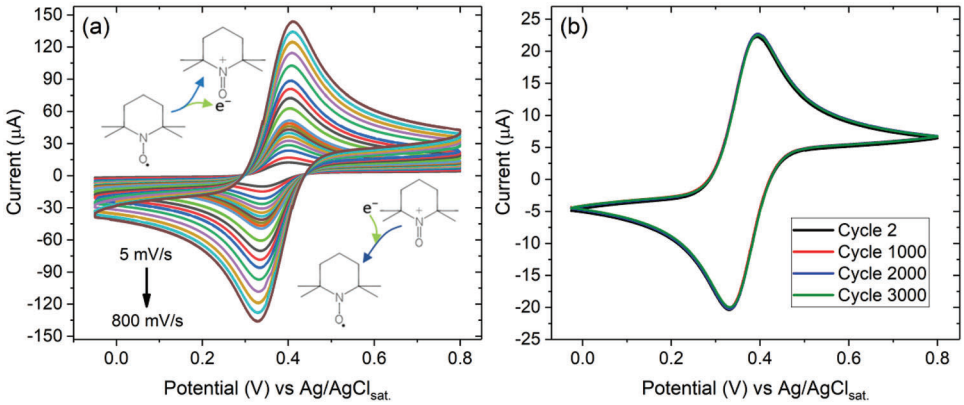

Figure 4. Electrochemical characterization of TEMPO in a three-electrode system. a) CVs of 10 mM TEMPO in 4 M LiTFSI solution measured at different scan rates. b) CV of 10 mM TEMPO in 4 M LiTFSI for 3000 cycles at 20 mV s^{-1}.

limiting active species ($TEMPO^+$) in this supporting electrolyte is 1.5 M. This solubility corresponds to a theoretical volumetric capacity of 40.2 Ah L^{-1} for the redox pair TEMPO/$TEMPO^+$.

2.4. Electrochemical Characterization of TEMPO Catholyte

Figure 4a shows the cyclic voltammetry (CV) of the system where the redox peaks associated with the reversible oxidation of nitroxide radical TEMPO to oxoammonium cation $TEMPO^+$ in 4 M LiTFSI aqueous electrolyte are clearly observed. The half-wave potential ($E_{1/2}$) was found to be 0.37 V versus Ag/$AgCl_{sat.}$ (0.57 V vs SHE). Noticeably, this value falls below the range exhibited by other reported TEMPO derivatives, (0.7–0.9 V vs SHE), although those are typically tested in less concentrated electrolytes.[13,17,18] To gain insights into this phenomenon, we conducted CV in solutions with increasing concentrations of LiTFSI. Remarkably, Figure S25, Supporting Information, shows a negative shift in the redox potential of TEMPO as the concentration of LiTFSI in the electrolytes increases. Specifically, it is shown that the redox potential of TEMPO in 1 M LiTFSI is 0.68 V versus SHE, this value is closely aligned with the typical potential range of reported TEMPO derivatives in electrolytes with comparable salt concentrations (0.7–0.9 V vs SHE).[13,17,18] The negative shift observed in Figure S25, Supporting Information, is consistent with our solubility tests and further substantiated by our molecular dynamics study. Those results showed that the increase in the LiTFSI concentration causes significant changes in the properties of the media and the solvation sphere of TEMPO, with enhanced intermolecular interactions between TEMPO and TFSI anions and higher coordination numbers. Since the energy required for the oxidation/reduction of TEMPO depends on the solvation sphere of TEMPO, the decreased redox potential can be attributed to such changes in the solvation sphere. This phenomenon has been recently reported by Zhu et al. in organic media, who also attributed this potential shift to the changes in the solvation energy of TEMPO and the related properties of the electrolyte (e.g., dielectric constant, ion pairing).[21] Although slightly lower than other TEMPO-derivatives, the redox potential of TEMPO in the selected supporting electrolyte (4 M LiTFSI) is still similar to ferrocene derivatives that are also commonly used as neutral pH catholytes in RFB.[22,23] A deep analysis of CV curves at different scan rates (Figure 4a) demonstrates that TEMPO has a highly reversible behavior in the 4 M LiTFSI aqueous electrolyte since it meets the different criteria for reversible systems; peak current ratio, potential peak separation, etc (see ESI for more details and Table S6 and Figure S26, Supporting Information). As expected, the linear relationship between peak current versus the square root of the scan rate (Ip vs $\nu^{1/2}$) (Figure S26c, Supporting Information) implies that the redox process is diffusion-controlled. The calculated diffusion coefficient according to the Randles–Sevcik equation is 8.05×10^{-7} cm^2 s^{-1}, which is in good agreement with the value obtained by applying the Levich method (8.90×10^{-7} cm^2 s^{-1}) (Figures S27 and S28, Supporting Information). This value is one order of magnitude lower than the one reported for different TEMPO derivatives (Table S7, Supporting Information) mainly due to the higher viscosity (9.4–11 cP, Table S8, Supporting Information) of this concentrated electrolyte which could limit the diffusivity of the redox species.

The kinetic rate constant (k^0) was determined to be 0.018 $cm^{-1}s$, which falls within the range of the fastest kinetics reported to date for functionalized TEMPO and other catholyte species (refer to Table S7, Supporting Information). This result highlights the fast kinetics of the redox TEMPO process, even at high concentrations of supporting salt (refer to Figure S29, Supporting Information, and EIS for details on the calculation). Interestingly, the excellent redox stability of TEMPO is anticipated in Figure 4b since the peak current, peak potential and shape of the CVs remained invariant over 3000 cycles.

2.5. Performance of TEMPO Catholytes in Symmetric Flow Cells

In order to assess the electrochemical performance of this newly developed TEMPO-based catholyte, symmetric cells with the same electrolyte composition in both compartments/tanks were initially assembled (see **Figure 5**a and Figure S30, Supporting Information). TEMPO-based electrolytes (0.1 and 0.5 M TEMPO at 50% state of charge (SOC) in 4 M LiTFSI) were investigated in unbalanced symmetric flow cells where an excess of volume (15%) was added in one of them to ensure a proper assessment of TEMPO stability. Initially, these TEMPO-based catholytes were

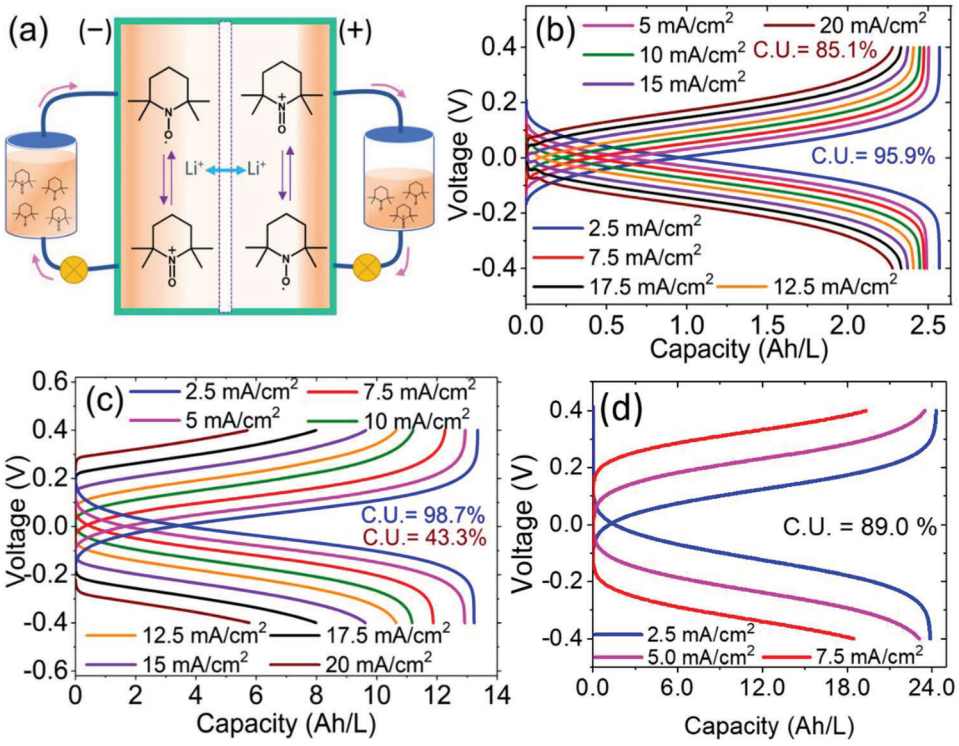

Figure 5. Electrochemical characterization of TEMPO symmetric flow cell system. a) Schematic illustration of a symmetric flow cell using TEMPO in LiTFSI electrolyte. b) Charge–discharge profiles of 0.1 M TEMPO in 4 M LiTFSI at different current densities. c) Charge–discharge profiles of 0.5 M TEMPO in 4 M LiTFSI at different current densities. d) Charge–discharge profiles of 1 M TEMPO in 4 M LiTFSI at different current densities. Theoretical capacity of the catholyte is 2.68, 13.4, and 26.8 Ah L^{-1} for 0.1, 0.5, and 1 M TEMPO catholytes, respectively.

galvanostatically tested at different current densities from 2.5 to 20 mA cm^{-2} (Figures 5b,c and Figures S31 and S32, Supporting Information, respectively). In both cases, adequate and quite flat plateaus appeared during the reversible oxidation-reduction processes of TEMPO catholyte (Figure 5b,c). As usually observed in any type of battery, the capacity decreases when increasing the current density due to the associated increased ohmic drop (Figure 5b,c). Remarkably, the electrolyte containing 0.1 M TEMPO exhibited a specific capacity of 2.57 Ah L^{-1} at a low current density of 2.5 mA cm^{-2} with a CE of 99.95%. This corresponds to a remarkable capacity utilization as high as 95.9% (Figure S31, Supporting Information). At a higher current density of 20 mA cm^{-2} a specific capacity of 2.28 Ah L^{-1} was obtained representing a high capacity utilization of 85.1% (with CE of 99.99%). Increasing by five times the concentration of active species, up to 0.5 M of TEMPO (Figure S32, Supporting Information), resulted in a specific capacity as high as 13.23 Ah L^{-1} at 2.5 mA cm^{-2} which entails a notably 98.7% capacity utilization (with CE of 99.11%). At higher current densities, the specific capacity decreased to 5.8 Ah L^{-1} (CE of 99.99%) representing a capacity utilization of 43.3%. This lower value of capacitive utilization at higher currents is likely due to the lower ionic conductivity of more concentrated TEMPO electrolyte (31.5 vs 16.10 mS cm^{-1} for 0.1 M TEMPO (50% SOC) and 0.5 M TEMPO (50% SOC), respectively). In order to demonstrate the viability of a highly concentrated catholyte, a catholyte containing 1 M TEMPO in 4 M LiTFSI was also formulated and characterized in symmetric cells at different current densities (Figure 5d). It is important to remark that this is the TEMPO-based catholyte with the highest concentration of active species tested in symmetric cells (Table S9, Supporting Information). This catholyte, with a theoretical volumetric capacity of 26.8 Ah L^{-1}, delivered a volumetric capacity as high as 23.85 Ah L^{-1} at 2.5 mA cm^{-2} (with CE of 98.3%) corresponding to a capacity utilization of 89%. Similar to previous symmetric cells, the higher overpotential at higher current densities caused a decrease in the obtained capacities (23.1 and 18.5 Ah L^{-1} at 5 and 7.5 mA cm^{-2}, respectively). This trend is slightly more pronounced than for catholytes with 0.1 and 0.5 M TEMPO due to the lower conductivity of this more concentrated catholyte (12.1 mS cm^{-1} for 1 M TEMPO (50% SOC).

After the galvanostatic test at different current densities, the current was fixed at ±10 mA cm^{-2} to evaluate the long-term cyclability of 0.1 and 0.5 M TEMPO electrolytes (**Figure 6**a,b). In the case of 0.1 M TEMPO-catholyte, the specific capacity was kept quite stable over cycling with a small decrease from 2.42 (at first cycle) to 2.17 Ah L^{-1} after 400 cycles (capacity retention ≈89.6%) maintaining CE >99% (see Figure 6a and Figures S33, Supporting Information). The corresponding capacity decay values over this cycling period were found to be as low as 0.026%/cycle and 1.152%/day. Due to the higher concentration of active species, the cycling test at ±10 mA cm^{-2} for the 0.5 M TEMPO catholyte lasted longer (41 days vs 9 days for 0.1 M TEMPO) for the same number of cycles (400 cycles, see Figure 6b). Nevertheless, the

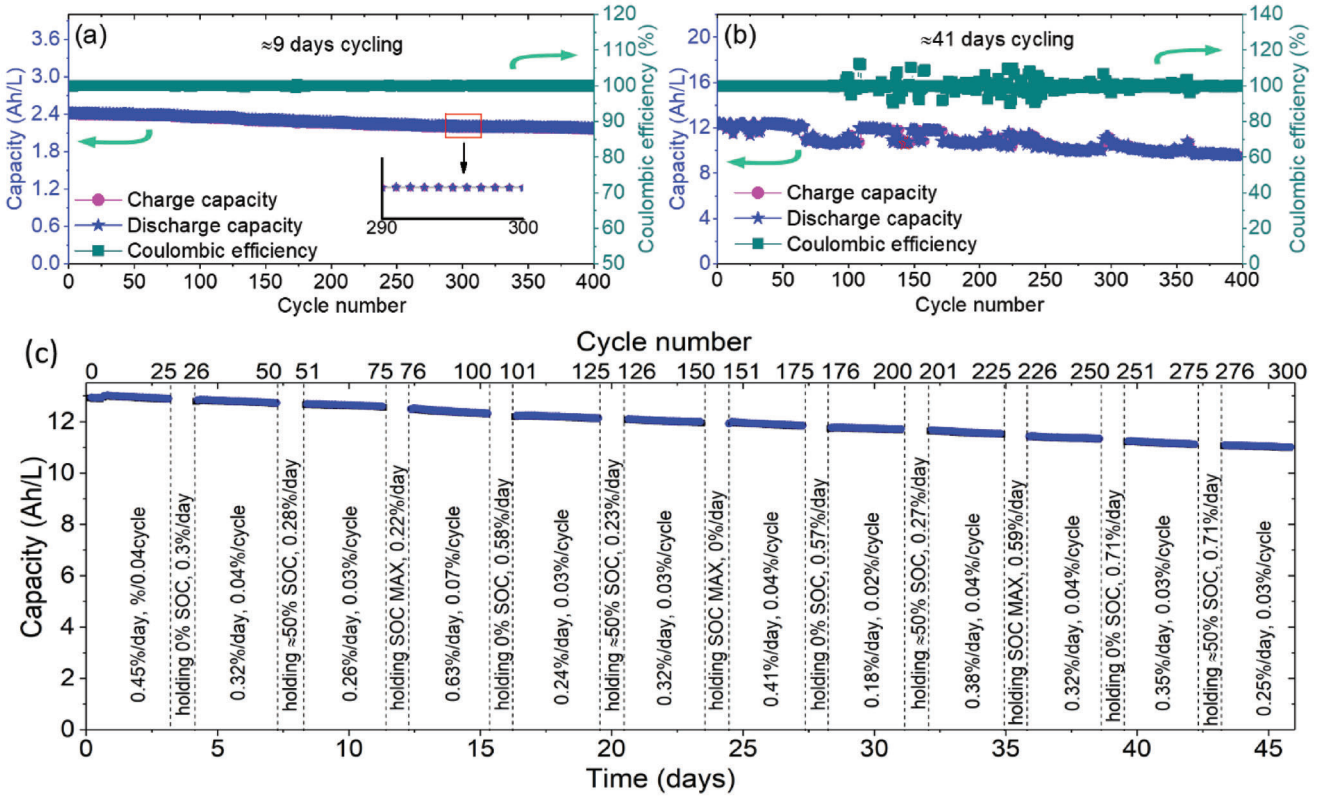

Figure 6. Cycling stability study of symmetric cells. a) 0.1 M TEMPO in 4 M LiTFSI at ±10 mA cm^{-2}. b) 0.5 M TEMPO in 4 M LiTFSI at ±10 mA cm^{-2}. The specific capacity is normalized by the volume of the catholyte (10 mL). Theoretical capacity of the catholyte is 2.68 and 13.4 Ah L^{-1} for 0.1 and 0.5 M TEMPO catholytes, respectively. c) The plot of charge and discharge capacities versus time (in days) for symmetric flow cell with 0.5 M TEMPO in 4 M LiTFSI as electrolyte. Cycles were performed at ±10 mA cm^{-2} by holding the cell at OCV at different SOC (0, ≈50%, and SOC$_{max}$) for 24 h every 25 cycles. Theoretical capacity of the catholyte is 13.4 Ah L^{-1}.

stability of the 0.5 M TEMPO catholyte was still very remarkable with a capacity retention of 77.3% and capacity decay values as low as 0.056%/cycle (0.552%/day) after 400 cycles (see Figure S34, Supporting Information). In fact, although the capacity decay per cycle is lower for 0.1 M TEMPO (0.026%/cycle vs 0.056%/cycle) the capacity decay per day is half than that for 0.1 M TEMPO (0.552%/day vs 1.152%/day). This is clearly seen in Figure S35, Supporting Information, which shows the cyclability test of 0.1 M TEMPO over 2600 cycles. This experiment lasted 47 days (comparable in time to the 400 cycles experiment for 0.5 M TEMPO) and the total capacity fading was 49%, quite larger than the 22.7% for 0.5 M TEMPO. These results evidenced the remarkable stability and suitability of 0.5 M TEMPO catholyte that was tested for almost 4 months (112 days) maintaining 58% of the initial capacity (Figure S36, Supporting Information). Interestingly, the stability of the symmetric cell with 0.5 M TEMPO is higher than for 0.1 M TEMPO. These findings can initially be perceived as "contraintuitive" as capacity fading caused by degradation typically increases as the concentration of active species increases. However, this seemingly contradictory outcome might be attributed to different factors. One factor is the marginal change in the maximum SOC achieved by both catholytes during the galvanostatic experiments. Another factor might be the different water content in both electrolytes. Since the progression of parasitic reactions depends on both the SOC and water content, even slight differences in these parameters between the two experiments might explain the observed differences in stability.

With the aim of a further evaluation of the stability of different oxidation states of TEMPO, a similar cycling study but incorporating resting periods of 24 h where the cell was maintained at OCV at different SOC (0%, ≈50%, and SOC$_{max}$) was performed. This study allows to identify the origin of the capacity decay that might be triggered by chemical and/or electrochemical decomposition of the TEMPO species (oxidized/reduced/mixture between them). Thus, the capacity fading was calculated at every interval of 25 cycles and also during the OCV periods aiming at distinguishing between the effect of the electrochemical cycling and the "storage time" at different SOC on the capacity retention. Figure 6c shows the long-term stability experiment for 0.5 M TEMPO catholyte including the capacity fading in each cycling and resting period (see also Figure S37, Supporting Information, for 0.1 M TEMPO). The total capacity retention was as high as 84.5% after the whole experiment corroborating the stability of this catholyte. During the galvanostatic cycling periods, the CE was>99.5%, and similar capacity decays were observed in all the cycling periods with an average capacity decay of 0.04%/cycle and 0.34%/day (Figure 6c). Interestingly, during the resting periods at OCV, regardless of the SOC, the average capacity decay was 0.36%/day, very similar to the one obtained

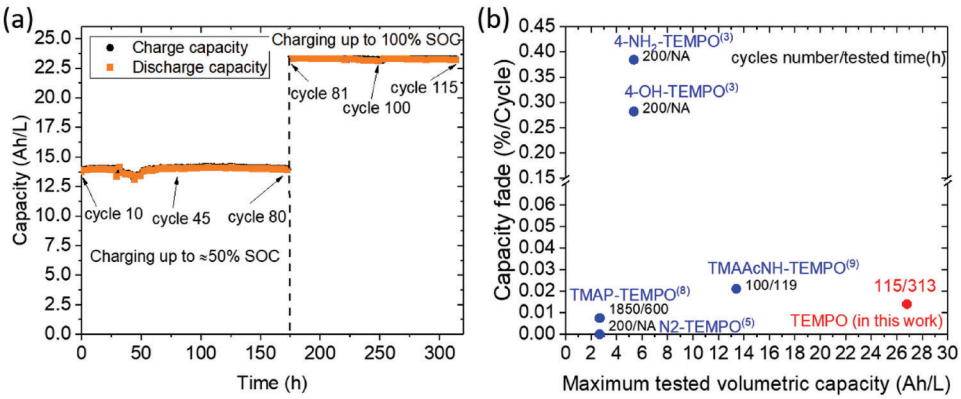

Figure 7. Cycling Stability study and comparison of 1 M TEMPO. a) Cycling stability of 1 M TEMPO symmetric cell. b) Comparison of the long-term cycling stability of state-of-the art catholytes based on TEMPO chemistry tested in symmetric cells.

during the electrochemical cycles. Moreover, very similar galvanostatic curves with similar capacity and no increased overpotential were obtained after these resting periods (see Figure S38, Supporting Information). Thus, the observed capacity decay was very low and almost constant over the whole experiment, including the cycling stages and the OCV resting periods at different SOCs. This minor but constant decay might be probably attributed to certain chemical degradation of TEMPO species that seems to be predominant over the electrochemical processes.

In the case of 1 M TEMPO catholyte, a long-cycling stability test was performed under potentiostatic conditions, using a symmetric cell configuration. During the first 80 cycles, the SOC of the catholyte was limited to ≈50%, whereas in the following cycles, it was allowed to reach the maximum SOC. **Figure 7**a shows that this catholyte was highly stable during the first cycling period at ≈50% SOC, with no observable capacity decay. During the second and more demanding testing period, the obtained initial capacity was as high as 23.6 Ah L^{-1}, very close to the theoretical one (corresponding to 88% capacity utilization). Moreover, the TEMPO catholyte exhibited excellent stability with very low capacity fading (0.014%/cycle and 0.082%/day) and high average Coulombic efficiency (CE = 99.65%) during cycling (Figure S39, Supporting Information). These results outperform the values achieved for some commonly used TEMPO derivatives, such as 4-OH-TEMPO[15] or 4-NH_2-TEMPO,[15] which show capacity fade rates more than ten times higher than the ones reported here (Figure 7b and Table S9, Supporting Information). Interestingly, the capacity fading of our non-functionalized TEMPO is similar or even lower than other TEMPO derivatives, such as TMAP-TEMPO[18] and TMAAcNH-TEMPO,[24] which were specifically designed to mitigate the degradation (see comparison in Figure 7b and Table S9, Supporting Information). Note that the volumetric capacity (theoretical and demonstrated) of this 1 M TEMPO catholyte is twice larger than for other reported TEMPO derivatives-based catholytes tested in symmetric cells. These results highlight the stability of the proposed TEMPO-based electrolyte and its applicability as a high-capacity catholyte for AORFB.

2.6. Electrochemical Performance of TEMPO/$(SPr)_2$ V Aqueous Redox Flow Battery

Finally, with the aim of demonstrating the applicability of the newly developed catholyte, we assembled a neutral-pH AORFB with TEMPO-based catholyte and an anolyte comprising 1,1′-bis(3-sulfonatopropyl)–4,4′-bipyridinium $(SPr)_2$ V. This commonly used viologen derivative also shows a remarkable solubility reaching 0.75 kg L^{-1} (1.53 M) in 4 M LiTFSI aqueous electrolyte. This points out that the solubilization strategy reported here is useful not only for non-functionalized TEMPO but also compatible with other common active species such as this viologen derivative. A detailed CV study of the $(SPr)_2$ V anolyte depicted in Figure S40, Supporting Information, revealed a fully reversible behavior in this supporting electrolyte with two reversible peaks centered at −0.7 and −1.1 V versus Ag/AgCl, assigned to the two redox processes ($(SPr)_2$ V $\overset{\pm e}{\leftrightarrow}$ $(SPr)_2V^-$ $\overset{\pm e}{\leftrightarrow}$ $(SPr)_2V^{2-}$). A detailed analysis of the reversibility of the first electron process is included in Table S10 and Figure S41, Supporting Information. The diffusion coefficient was calculated by Randles–Sevcik (Figure S42, Supporting Information) and Levich (Figure S43, Supporting Information) methods obtaining the same value of 3.6×10^{-7} cm^2 s^{-1}. This value is one order of magnitude lower than the reported for other viologen derivatives probably due to the higher viscosity of the 4 M LiTFSI aqueous solution. On the other hand, the calculated kinetic rate constant was 0.022 $cm^{-1}s$ (see Figure S44, Supporting Information), which is similar to or even higher than those reported for other viologen derivatives in common supporting electrolytes.[25] This points out the fast kinetics of the selected viologen derivative in this LiTFSI-based supporting electrolyte. Once the appropriate electrochemical properties of the anolyte were confirmed, the feasibility of the TEMPO/$(SPr)_2$ V aqueous organic RFB, with a theoretical OCV of 1.08 V according to the CV of the individual electrolytes (**Figure 8**a), was addressed in a full battery.

A schematic representation of the TEMPO/$(SPr)_2$ V flow battery and the reactions of TEMPO and $(SPr)_2$ V are presented in Figure 8b,c. Figure 8d shows the charge–discharge profiles at different current densities (from 7.5 to 20 mA cm^{-2}) showing good electrochemical performance with excellent CE and an average

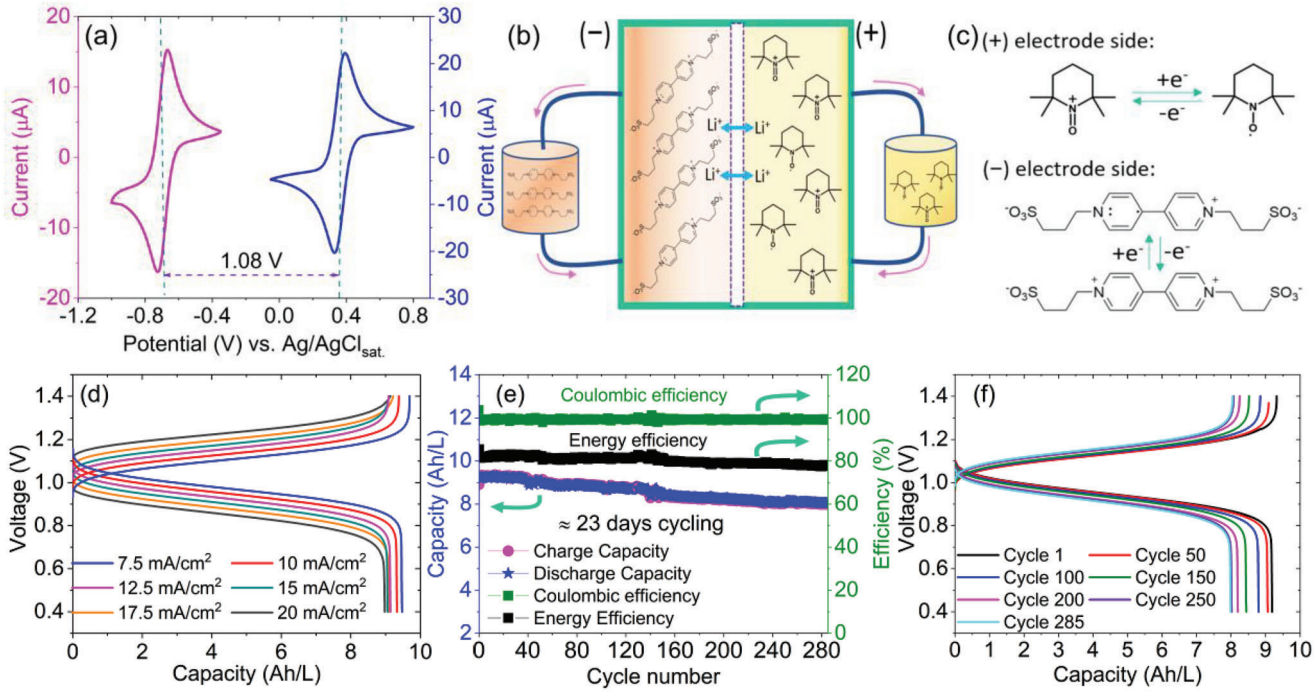

Figure 8. Electrochemical characterization of TEMPO/$(SPr)_2$ V redox flow battery. a) CV measured in 10 mM TEMPO in 4 M LiTFSI electrolyte (blue trace) and 10 mM $(SPr)_2$ V in 4 M LiTFSI electrolyte (pink trace) at 20 mV s^{-1}. b,c) Schematic representation of TEMPO/$(SPr)_2$ V redox flow battery and their redox reaction. d) Charge–discharge profiles at different current densities (7.5–20 mA cm^{-2}). e) Cycle performances at 10 mA cm^{-2}. f) Charge–discharge profiles of selected cycles during cycling test at 10 mA cm^{-2}. The provided capacity is normalized by the total volume of the catholyte (theoretical capacity = 13.4 Ah L^{-1}).

cell voltage of 0.96 V, close to the theoretical one at 7.5 mA cm^{-2}. Moreover, the reached capacity was 9.47 Ah L^{-1} corresponding to a capacity utilization as high as 70.7% at 7.5 mA cm^{-2}. This capacity slightly decreased to 9 Ah L^{-1} when increasing the current to 20 mA cm^{-2}. Note that, similar to other viologens anolytes, just the first electron exchange reaction contributed to the capacity. Accessing the second one was not feasible due to the limited solubility of the dianion reduced species ($(SPr)_2V^{2-}$) that caused clogging of the porous electrode and pumping limitations due to internal overpressure (see Figure S45, Supporting Information).

In order to evaluate the long-term stability, the battery was galvanostatically cycled at 10 mA cm^{-2} over 285 cycles. As presented in Figure 8e, the initial capacity was 9.3 Ah L^{-1}, slightly decreasing over cycling with an average CE of 99.5% throughout all cycles (see Figure S46, Supporting Information). This value corresponds to a capacity utilization of 69%, in the same range as AORFB with similar chemistries (Table S11, Supporting Information).[13,17,19] Figure 8f depicts the charge–discharge profiles of selected cycles showing a slight decrease in capacity and quite stable overpotentials. This long-cycling test evidences a low capacity decay rate of 0.048%/cycle or 0.60%/day with a total capacity retention of 86.4% over the whole period (552 h). The capacity retention per day exhibited by this AORFB (over a very long experiment) and the energy efficiency (EE = 82%) are among the highest reported when compared with TEMPO & viologen-based AORFB (see Table S11, Supporting Information). In addition, it should be pointed out that this long-term cycling test (552 h, ≈23 days) is one of the longest reported in the literature. Thus, the proposed aqueous TEMPO-based catholyte is confirmed as a feasible high-capacity, highly efficient, and stable catholyte for ARFB. The newly developed approach to promote the solubility of non-functionalized TEMPO in aqueous supporting electrolytes, simply by selecting the appropriate supporting salt, has been demonstrated as an effective strategy. This breakthrough approach might be applied to other redox species, thereby opening up new possibilities for the development of AORFB.

3. Conclusion

This work demonstrates for the first time, the feasibility of using non-functionalized TEMPO as an efficient aqueous catholyte for AORFB. Previously, the utilization of pristine TEMPO in AORFB was hindered due to its insolubility in water (0.07 M), which required the synthesis of soluble TEMPO derivatives prior to their use in AORFB. Here, a new solubilization strategy has been developed, resulting in an unprecedented solubility of 5.6 M (9.4 kg L^{-1}) of pristine TEMPO in a 5 M LiTFSI aqueous solution. Notably, the solubility of the oxidized species ($TEMPO^+$), which is often overlooked in the literature, was also investigated, reaching a remarkable value of 2.3 M in 5 M LiTFSI electrolyte. Molecular dynamics simulations revealed a unique intermolecular interaction between TFSI anion and TEMPO (and $TEMPO^+$), promoting a change in their coordination environment incorporating more $TFSI^-$ and expelling other TEMPO molecules from its coordination shell, enabling their high solubility in the supporting electrolyte. The computational studies corroborate the experimental results, demonstrating the dependence of TEMPO and $TEMPO^+$ solubility on the LiTFSI concentration.

Due to the superior physicochemical properties of 4 M LiTFSI solution, this was selected as the supporting electrolyte, despite the slightly lower solubilities of TEMPO and $TEMPO^+$ (5.5 and 1.5 M, respectively). The TEMPO-based catholytes, containing 0.1, 0.5, and 1 M TEMPO in 4 M LiTFSI were tested in symmetric cells, exhibiting high reversible electrochemical activity and robust performance with a demonstrated volumetric capacity as high as 23.85 Ah L^{-1} for 1 M TEMPO catholyte (89% of the theoretical capacity). Long-term cyclability experiments revealed the high (electro)chemical stability of TEMPO-based catholytes, with 1 M TEMPO exhibiting high Coulombic efficiency (>99.5%) and a capacity fading as low as 0.082%/day over cycling. Finally, the reliability of this catholyte was demonstrated by pairing it with a viologen derivative-based anolyte which showed also compatibility with the LiTFSI electrolyte. The resulting TEMPO/$(SPr)_2$ flow battery, with an OCV of 1.08 V, exhibited efficient and stable performance, with high CE (>99%) and 70.7% capacity utilization at 7.5 mA cm^{-2}. The long-term cycling test (552 h, 285 cycles) at 10 mA cm^{-2} demonstrated the high stability of the AORFB, which exhibited a low capacity fade rate of 0.60%/day or 0.048%/cycle and high energy efficiency (82%).

The demonstrated approach involving the selection of an appropriate supporting electrolyte and considering the specific interactions between TEMPO and TFSI anion has resulted in the successful application of a highly soluble, non-functionalized TEMPO as a suitable catholyte for AORFB. This achievement is significant as it eliminates the need for synthesizing soluble TEMPO derivatives specifically for AORFB. We envision that this novel strategy to boost the solubility of active species might be extended to other families of organic molecules, employing more affordable supporting salts and reducing the required concentration of salts. This, in turn, will offer promising prospects for the development of cost-effective and reliable AORFB.

4. Experimental Section

Synthesis of TEMPO-TFSI and SPr_2V: The 2,2,6,6-tetramethylpiperidin-1-oxoammonium bis(trifluoromethane)sulfonamide (TEMPO-TFSI) was synthesized following the procedure described elsewhere with some modifications (see additional details in the Supporting Information).[26] A bright yellow solid in 83% yield was obtained as the final product and characterized with NMR spectroscopy in CD_3CN (See Figures S1–S3, Supporting Information).

1,1′-Bis(3-sulfonatopropyl)–4,4′-bipyridinium (SPr_2V) was prepared according to a modified procedure of a reported method (see additional details in the Supporting Information).[27] The product (SPr_2V) was obtained as a white solid in 90% yield (11.22 g) and characterized with NMR spectroscopy in D_2O (see Figures S4 and S5, Supporting Information).

Solubility Test: The solubility of TEMPO was determined in 1 M concentration of different Li-based salts such as Li_2SO_4, $LiClO_4$, $LiNO_3$, LiCl, LiTFSI, and NaTFSI. Then, the solubility of TEMPO and TEMPO-TFSI was also evaluated in 1, 2, 3, 4, and 5 M LiTFSI aqueous solutions, respectively. A small amount of the solute (either TEMPO or TEMPO-TFSI) was first weighed. Then, successive additions (with micropipettes) of a known volume of supporting electrolyte were added under stirring until the complete dissolution of the solute. Between each addition of supporting electrolyte, the sample was allowed to stand for 5 min approximately until complete dissolution was observed. Once solutes reached their solubility limit, the mass, density, and volume of the saturated solution were determined, and the solubility values were calculated. Solubility values were expressed as molarity (M) and as kg L^{-1} which refers to kg of solute in L of aqueous supporting electrolyte according to Equations (1) and (2)

$$\text{Solubility}\left(\frac{\text{mol}}{\text{L}}\right) = \frac{\text{mol of solute}}{\text{Liters of solution}} \quad (1)$$

$$\text{Solubility}\left(\frac{\text{kg}}{\text{L}}\right) = \frac{\text{kg of solute}}{\text{Liters of solvent}} \quad (2)$$

Theoretical Calculations: Molecular dynamics simulations were carried out using the GROMACS 2020 software.[28] The CHARMM36 forcefield[29] was used for the description of nitroxide radical (TEMPO) and the supporting salts with the exception of TFSI- anion, which was modeled using a specific ionic-liquids forcefield: CL&P forcefield.[30] Water molecules were modeled with the SPC/E forcefield.[31,32] Additional details are described in the Supporting Information.

Electrolytes Characterization: The ionic conductivity of LiTFSI-based supporting electrolytes was obtained using a Hamilton conducell 4US Arc Sensors.

CVs of redox-active electrolytes were carried out using a Biologic VMP multichannel potentiostat in a three-electrode cell configuration with a glassy carbon of 3 mm in diameter, platinum wire, and Ag/AgCl (sat. NaCl) as working electrode, counter electrode, and reference electrode, respectively. Solutions of 10 mM TEMPO in 4 M LiTFSI and 10 mM $(SPr)_2$ V in 4 M LiTFSI were prepared individually and used as electrolytes. CVs were performed at different scan rates from 5 to 800 mV s^{-1} after deoxygenating the electrolytes bubbling argon for 10 min. Linear sweep voltammetry (LSV) studies were carried out with the same 3-electrode configuration and the same size of electrodes using a rotator system RRDE-3A from ALS Co and applying rotating speeds from 300 to 2700 rpm and using a scan rate of 5 mV s^{-1}. Analysis of the reversibility and determination of kinetic parameters of the redox active species (i.e., TEMPO or $(SPr)_2$ V) is detailed in the Supporting Information (see Section S6, Supporting Information).

Assembly of Electrochemical Flow Cells: All electrochemical flow cells (symmetric cells and full RFBs) were assembled using filter-pressed reactors. Nafion N117, expanded graphite (SGL Carbon), and carbon felt with a 9 cm^2 geometric area were used as cation exchange membranes, supporting current collectors, and current collectors, respectively. The Nafion N117 membranes were pretreated by immersion in a blank electrolyte (4 M LiTFSI) for at least 48 h and the graphite-felt electrodes were pretreated at 500 °C in an air atmosphere for 2 h. A peristaltic pump (MasterFlex L/S), MaxterFlex precision tubes of Tygon (1.6 mm of diameter), and MaterFlex pump heads were used to provide a flow rate of 20 mL min^{-1}.

Electrochemical Characterization of Symmetric Electrochemical Cells: Solutions of the desired concentration (0.1, 0.5, or 1 M) were prepared individually for TEMPO and TEMPO-TFSI in 4 M TFSI. For the initial TEMPO-based catholytes (0.1, 0.5, or 1 M) at 50% SOC, equal volumes of each solution (TEMPO and TEMPO-TFSI) at the desired concentrations (0.1, 0.5, or 1 M) were mixed. These 50% SOC electrolytes were investigated in an unbalanced symmetric flow. In the case of 0.1 and 0.5 M TEMPO 10 mL of electrolyte was used in the limiting compartment and 15% excess volume in the non-limiting compartment. In the case of 1 M TEMPO, 9 mL was used for the limiting compartment and a 1 mL excess was added to the non-limiting tank

The two TEMPO-based electrolytes (0.1 and 0.5 M TEMPO at 50% SOC in 4 M LiTFSI) were initially galvanostatically tested in compositionally symmetric cells using different density currents (from ±2.5 to ±20 mA cm^{-2} with increments of 2.5 mA cm^{-2}) and a voltage cut-off of ±400 mV. After that, the symmetric cells were subjected to long-term galvanostatic experiments at a fixed current of ±10 mA cm^{-2}. In the case of the symmetric cell at 1 M TEMPO, the cyclability test was performed under potentiostatic conditions holding a voltage of ±400 mV. Cycles at ≈50% SOC were limited by time and cycles at 100% SOC were limited by current

density cut-off of ±1 mA cm^{-2}.[33] The theoretical capacity and the capacity utilization were calculated according to Equations (3) and (4)

$$\text{Theoretical Capacity } \left(\frac{\text{Ah}}{\text{L}}\right) = \frac{n \times C \times F}{3600} \quad (3)$$

$$\text{Capacity Utilization } (\%) = \frac{\text{Capacity}}{\text{Theoretical Capacity}} \times 100 \quad (4)$$

The capacity retention and the capacity decay were calculated according to Equations (5–7)

$$\text{Capacity decay } \left(\frac{\%}{\text{cycle}}\right) = \frac{\frac{\text{Initial capacity}-\text{Final capacity}}{\text{Initial capacity}} \times 100}{\text{number of cycles}} \quad (5)$$

$$\text{Capacity decay } \left(\frac{\%}{day}\right) = \frac{\frac{\text{Initial capacity}-\text{Final capacity}}{\text{Initial capacity}} \times 100}{\text{number of days}} \quad (6)$$

$$\text{Capacity retention } (\%) = 100 - \%\text{Capacity decay} \quad (7)$$

To further study the stability of the catholyte, another two symmetric cells with freshly prepared electrolytes (0.1 and 0.5 M TEMPO at 50% SOC in 4 M LiTFSI) were galvanostatically cycled at constant ±10 mA cm^{-2} during long cycling. Every 25 cycles, resting periods of 24 h holding the system at OCV at different estimated SOC (0%, ≈50%, and SOC_{max}), were applied to investigate the effect of these resting periods in the degradation of the catholyte. SOC_{max} refers to the maximum reached SOC (in the range of 70–90%) which differs from 100% due to the mass transport limitations derived from the galvanostatic cycling conditions. The pumps remained turned on, maintaining the same flow rate throughout the entire test including the resting periods. All the tests were performed using a Biologic VMP multichannel potentiostat bubbling argon to the electrolytes 20 min prior to the experiments.

Electrochemical Characterization of $(SPr)_2$ V/TEMPO Full RFB: TEMPO-based catholyte (10 mL of 0.5 M TEMPO in 4 M LiTFSI) was paired with a $(SPr)_2$V-based anolyte (23 mL of 0.25 M $(SPr)_2$ V in 4 M LiTFSI) in a full RFB (20% anolyte capacity excess). The $(SPr)_2$ V/TEMPO full RFB was galvanostatically charged–discharged at different current densities (from 7.5 to 20 mA cm^{-2} with increments of 2.5 mA cm^{-2} and voltages cut-off of 0.4 and 1.4 V, respectively). In order to assess the long-term stability of the full RFB, long-term galvanostatic cycles were performed at 10 mA cm^{-2}. All the tests were performed in an MBraun glove box in the absence of oxygen (<1 ppm O_2) using a Biologic VMP multichannel potentiostat.

Supporting Information

Supporting Information is available from the Wiley Online Library or from the author.

Acknowledgements

The authors acknowledge the financial support by the Spanish Government (PID2021-124974OB-C21, PID2021-124974OB-C22, and TED2021-129378B-C22), the Comunidad de Madrid (TALENTO grant 2017-T1/AMB-5264 and 2021–5A/AMB-20946), as well as the European Union through the MeBattery, Light-cap and MFreeB projects. MeBattery and Light-cap received funding from the European Innovation Council (grant Agreement no. 101046742 and 101017821) and the MFreeB project received funding from the European Research Council (ERC) under the European Union's Horizon 2020 (grant agreement No. 726217). The authors acknowledge the computing facilities of CSUC for providing resources that contributed to the research results reported within this paper.

Conflict of Interest

The authors declare no conflict of interest.

Data Availability Statement

The data that support the findings of this study are openly available in ZENODO at https://zenodo.org/deposit/8307920, reference number DOI: 10.5281/zenodo.8307920.

Keywords

2,2,6,6-tetramethylpiperidine-1-oxyl (TEMPO), aqueous redox flow batteries, intermolecular interaction, molecular dynamics, organic redox molecules, solubility, symmetric cells

Received: June 19, 2023
Revised: August 11, 2023
Published online:

[1] P. Alotto, M. Guarnieri, F. Moro, *Renewable Sustainable Energy Rev.* **2014**, *29*, 325.
[2] E. Sánchez-Díez, E. Ventosa, M. Guarnieri, A. Trovò, C. Flox, R. Marcilla, F. Soavi, P. Mazur, E. Aranzabe, R. Ferret, *J. Power Sources* **2021**, *481*, 228804.
[3] D. G. Kwabi, K. Lin, Y. Ji, E. F. Kerr, M. A. Goulet, D. De Porcellinis, D. P. Tabor, D. A. Pollack, A. Aspuru-Guzik, R. G. Gordon, M. J. Aziz, *Joule* **2018**, *2*, 1894.
[4] F. Zhong, M. Yang, M. Ding, C. Jia, *Front. Chem.* **2020**, *8*, 451.
[5] Z. Li, T. Jiang, M. Ali, C. Wu, W. Chen, *Energy Storage Mater.* **2022**, *50*, 105.
[6] K. Gong, Q. Fang, S. Gu, S. F. Y. Li, Y. Yan, *Energy Environ. Sci.* **2015**, *8*, 3515.
[7] C. DeBruler, B. Hu, J. Moss, X. Liu, J. Luo, Y. Sun, T. L. Liu, *Chem* **2017**, *3*, 961.
[8] C. Zhang, Z. Niu, Y. Ding, L. Zhang, Y. Zhou, X. Guo, X. Zhang, Y. Zhao, G. Yu, *Chem* **2018**, *4*, 2814.
[9] Y. Ding, Y. Li, G. Yu, *Chem* **2016**, *1*, 790.
[10] Z. Zhou, L. Liu, *Curr. Org. Chem.* **2014**, *18*, 459.
[11] X. Wei, W. Xu, M. Vijayakumar, L. Cosimbescu, T. Liu, V. Sprenkle, W. Wang, *Adv. Mater.* **2014**, *26*, 7649.
[12] B. J. Bergner, A. Schürmann, K. Peppler, A. Garsuch, J. Janek, *J. Am. Chem. Soc.* **2014**, *136*, 15054.
[13] T. Liu, X. Wei, Z. Nie, V. Sprenkle, W. Wang, *Adv. Energy Mater.* **2016**, *6*, 1501449.
[14] A. Orita, M. G. Verde, M. Sakai, Y. S. Meng, *J. Power Sources* **2016**, *321*, 126.
[15] W. Zhou, W. Liu, M. Qin, Z. Chen, J. Xu, J. Cao, J. Li, *RSC Adv.* **2020**, *10*, 21839.
[16] F. R. Brushett, M. J. Aziz, K. E. Rodby, *ACS Energy Lett.* **2020**, *5*, 879.
[17] T. Janoschka, N. Martin, M. D. Hager, U. S. Schubert, *Angew. Chem., Int. Ed.* **2016**, *55*, 14427.
[18] Y. Liu, M. A. Goulet, L. Tong, Y. Liu, Y. Ji, L. Wu, R. G. Gordon, M. J. Aziz, Z. Yang, T. Xu, *Chem* **2019**, *5*, 1861.
[19] B. Hu, M. Hu, J. Luo, T. L. Liu, *Adv. Energy Mater.* **2022**, *12*, 2102577.
[20] H. J. C. Berendsen, D. van der Spoel, R. van Drunen, *Comput. Phys. Commun.* **1995**, *91*, 43.
[21] F. Zhu, Y. Zou, L. Hua, X. Peng, W. Zhang, *Electrochem. Commun.* **2022**, *142*, 107374.
[22] B. Hu, C. DeBruler, Z. Rhodes, T. L. Liu, *J. Am. Chem. Soc.* **2017**, *139*, 1207.

[23] E. S. Beh, D. De Porcellinis, R. L. Gracia, K. T. Xia, R. G. Gordon, M. J. Aziz, *ACS Energy Lett.* **2017**, *2*, 639.
[24] H. Fan, W. Wu, M. Ravivarma, H. Li, B. Hu, J. Lei, Y. Feng, X. Sun, J. Song, T. L. Liu, *Adv. Funct. Mater.* **2022**, *32*, 2203032.
[25] V. Singh, S. Kim, J. Kang, H. R. Byon, *Nano Res.* **2019**, *12*, 1988.
[26] F. Carlet, G. Bertarini, G. Broggini, A. Pradal, G. Poli, *Eur. J. Org. Chem.* **2021**, *2021*, 2162.
[27] J. Luo, B. Hu, C. Debruler, Y. Bi, Y. Zhao, B. Yuan, M. Hu, W. Wu, T. L. Liu, *Joule* **2019**, *3*, 149.
[28] M. J. Abraham, T. Murtola, R. Schulz, S. Páll, J. C. Smith, B. Hess, E. Lindahl, *SoftwareX* **2015**, *1–2*, 19.
[29] K. Vanommeslaeghe, A. D. MacKerell, *Biochim. Biophys. Acta, Gen. Subj.* **2015**, *1850*, 861.
[30] J. N. Canongia Lopes, A. A. H. Pádua, *Theor. Chem. Acc.* **2012**, *131*, 1129.
[31] H. J. C. Berendsen, J. R. Grigera, T. P. Straatsma, *J. Phys. Chem.* **1987**, *91*, 6269.
[32] S. Chatterjee, P. G. Debenedetti, F. H. Stillinger, R. M. Lynden-Bell, *J. Chem. Phys.* **2008**, *128*, 124511.
[33] M.-A. Goulet, M. J. Aziz, *J. Electrochem. Soc.* **2018**, *165*, A1466.